Spatiotemporal Analysis by Deep Learning of Gait Signatures From Floor Sensors

Abdullah S. Alharthi, Alexander J. Casson, *Senior Member, IEEE*, and Krikor B. Ozanyan, *Senior Member, IEEE*

***Abstract*—The recognition of gait pattern variation is of high importance to various industrial and commercial applications, including security, sport, virtual reality, gaming, robotics, medical rehabilitation, mental illness diagnosis, space exploration, and others. The purpose of this paper is to study the nature of gait variability in more detail, by identifying gait intervals responsible for gait pattern variations in individuals, as well as between individuals, using cognitive demanding tasks. This work uses deep learning methods for sensor fusion of 116 plastic optical fiber (POF) distributed sensors for gait recognition. The floor sensor system captures spatiotemporal samples due to varying ground reaction force (GRF) in multiples of up to 4 uninterrupted steps on a continuous 2 x 1 m area. We demonstrate classifications of gait signatures, achieving up to 100% F1-score with Convolutional Neural Networks (CNN), in the context of gait recognition of 21 subjects, with imposters and clients. Classifications under cognitive load, induced by 4 different dual tasks, manifested lower F1-scores. Layer-Wise Relevance Propagation (LRP) methods are employed to decompose a trained neural network prediction to relevant standard events in the gait cycle, by generating a "heat map" over the input used for classification. This allows valuable insight into which parts of the gait spatiotemporal signal have the heaviest influence on the gait classification and consequently, which gait events, such as heel strike or toe-off, are mostly affected by cognitive load.**

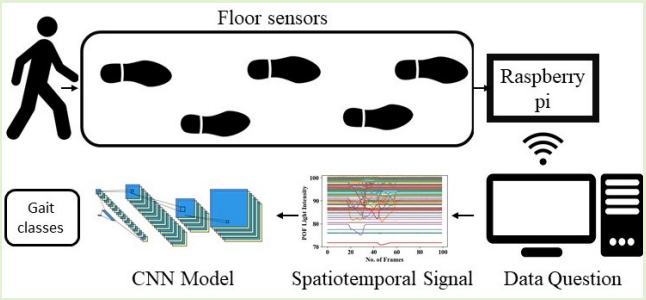

***Index Terms*— Deep convolutional neural networks (CNN), cognitive load, ground reaction force (GRF), sensors fusion, interpretable neural networks.**

I. Introduction

GAIT recognition has been intensively studied in recent years for the best achievable accuracy in distinguishing a certain target case in a plethora of applications, e.g. in healthcare, biometrics [1] and authentication for surveillance and forensics [2]. Conventional gait sensing technologies are borrowed from well populated research areas, such as image and video recognition, wearable sensors [1], and speech recognition [3]. Previous studies proposed cameras to record video sequence of the body motion [4], wearable sensors to acquire the limbs' trajectories and body posture [5], or microphones to capture the sound of footsteps [3]. These methods generally perform well, however the quality of data embodying the spatial and temporal aspects of gait is affected by clothing's conditions, angles in video sequences, the limitation in the format of the captured signals in wearable sensors and motion capturing systems, or the presence of other environment acoustic noise in the captured footstep sound.

An alternative approach is to use force plates to acquire the ground reaction force (GRF) [6], considering that the interaction with the walking surface is at the point of contact with the environment, which cannot be avoided or modified at will. However, force plates cover small areas, and the user may often need to artificially modify their gait aiming to step at a certain location. A preferable choice for GFR sensing of gait would be a large area unobtrusive floor sensor system, delivering high resolution spatiotemporal signals, which requires minimal (if any) cooperation or special attention by the user and allows long period, continuous data capture [1].

Due to the ambulatory nature of human gait, the environment varies, directly or indirectly rendering an individual's gait inconsistent. A growing body of studies demonstrates that attention demanding tasks alters the walking pattern in all healthy individuals in response to dual tasking, and gait should not be regarded as an automated motor activity that receives minimal higher-level cognitive input [7], [8]. Certainly, deliberate gait is essential for humans to navigate within often complex environment's while concurrently execute cognitive

Manuscript received March 25, 2021; accepted April 30, 2021. Date of publication May 7, 2021; date of current version July 30, 2021. The work of Abdullah S. Alharthi was supported by the Government of Saudi Arabia. The associate editor coordinating the review of this article and approving it for publication was Dr. Ying Zhang. *(Corresponding author: Abdullah S. Alharthi.)*

The authors are with the Department of Electrical and Electronic Engineering, The University of Manchester, Manchester M13 9PL, U.K. (e-mail: abdullah.alharthi@manchester.ac.uk; alex.casson@manchester.ac.uk; k.ozanyan@manchester.ac.uk).

Digital Object Identifier 10.1109/JSEN.2021.3078336

demanding tasks while walking to reach a desired destination. The progressive adjustment of gait is regarded as a way for individuals to minimize the energy cost during the gait cycle, while walking based on environment's burdens [9], [10]. Humans continuously optimize energy cost in real-time, even if the energy savings while walking are small [11]. Thus, the energy conservation drives changes in gait dynamics, based on cognitive processing of information.

Furthermore, person's emotional state, such as pride, happiness, fear and anger, are found to affect gait [12]. However, the inconsistency of gait can be advantageous for gait biometric verification since gait under cognitive load would carry a unique signature due to individual variations in the cost of processing cognitive information. Another possible scenario is to detect and characterize cognitive decline with age e.g. facilitated by floor-embedded inexpensive sensor systems. Such a scenario is relevant to clinical diagnosis of mobility decline and impairments in gait and postural control due to natural aging process [13]; fall risk [14], [15] as well as mental decline, e.g. Alzheimer's disease, dementia with Lewy bodies, vascular dementia, Parkinson's disease [16].

This work utilizes floor sensors and implements an original protocol for recording gait under cognitive load ("dual tasks"). For the purpose, a healthy subject's natural gait is used as a control recording for the acquisition and processing of gait data under a cognitively demanding task. This work addresses in a novel way a number of challenges, identified in literature and by own observations, pertaining to the physical sensing layer, as well as the data processing. Signals are recorded with an original floor sensor system, specially designed, and built for optimal spatiotemporal sampling with multiple plastic optical fiber (POF) distributed sensors [17]–[20]. Multiple sensor fusion is achieved by deep learning with convolutional neural networks (CNN) used to classify subjects' gait. Explainable [21] CNN methodology is applied to relate achieved classifications to the input data, allowing visually observable gait events to be identified as most relevant for a certain class. The explainable methodology is based on the existing well-defined cyclic locomotion patterns in healthy human gait, allowing to query what part of the gait cycle is essential for recognition and what are the parts acting as a background (irrelevant for the classification) by CNN processing. Layer-Wise Relevance Propagation (LRP) techniques are applied in this work to interpret the CNNs prediction and identifying the gait events with largest weight for gait recognition.

The rest of the paper is organized as follows. After introducing the necessary background in section II and methodology in section III, the experiments and results are presented in section IV. Substantial discussion of the results is included in section V, followed by conclusions in section VI.

II. Background

A. Deep CNNs and LRP

The deep CNNs core building block is the convolution operator, with the term 'deep' referring to the number of layers. A convolution layer learns a high level of abstraction and pattern by applying convolution operations, with the aim to extract features' representations automatically. A convolution operation C_s for layer s, with an input x_i and kernel l, can be expressed as:

$$C_S = x_i * l_i = \sum_{d=0}^{N-1} x\,(d) * l(i-d) \tag{1}$$

Here d and $*$ denote correspondingly the iteration index and the element-wise multiplication. The deep CNNs utility is based on the ability to model complex relationships between inputs and outputs and find patterns in divergent data with high background levels. Widely researched applications, presenting weak features on high background, are face [22], text [23] and speech recognition [24]. Since gait is characterized by events occurring naturally in all healthy humans, a comparatively small number of weakly manifested features can be picked up to make a classification in biometrics or indicate a health condition by detecting spatiotemporal deviations from gait previously categorized as "normal" for a specific individual.

For most data classification cases a nonlinear deep ANN model acts as a black box, since the reasons as to why the models reached such decisions are not straightforward to trace to physical events. LRP [21] is a backward propagation method applied in interpretable deep learning, which identifies which parts of the ANN input vector carry most weight in the model prediction. This method has proven to be successful in a number of applications [22]–[24] to identify the divergent features for a model to make prediction, thus LRP is promising for unravelling the spatiotemporal signal and scrutinizing gait events, to the benefit of developing a certain application, e.g. aid to clinical assessment or to biometric verification.

B. iMAGiMAT System

The iMAGiMAT footstep imaging system is an original Photonic Guided-Path Tomography floor sensor head [17]–[20]). It can record unobtrusively temporal samples from a number of strategically placed distributed POF sensors on top of a deformable underlay of a commercial retail floor carpet. Each sensor comprises of low cost POF (step-index PMMA core with fluorinated polymer cladding and polyethylene jacket, total diameter 1mm, NA = 0.46) terminated with a LED (Multicomp OVL-3328 625nm) at one end and a photodiode (Vishay TEFD4300) at the other. The sensors constitute a carefully designed set to allow collaborative sensor fusion and deliver spatiotemporal sampling adequate for discerning gait events. The 1m × 2m area system is managed by 116 POF sensors, arranged in three parallel plies, sandwiched between the carpet top pile and the carpet underlay: a lengthwise ply with 22 POF sensors at 0° angle to the walking direction and two independent plies, each consisting of 47 POF sensors, arranged diagonally at 60° and −60° respectively (see [17], fig. 6 therein).

The electronics is contained in a closed hard-shell periphery at carpet surface level, and is organised in 8-channel modules: LED Driver boards as well as input transimpedance amplifier boards to receive the data and send it to a CPLD (Complex programmable logic device) to reformat the data for processing by a Raspberry pi single board computer for export via Ethernet/WiFi.

The operational principle of the system is based on recording the deformation caused by the GRF variations, as bending

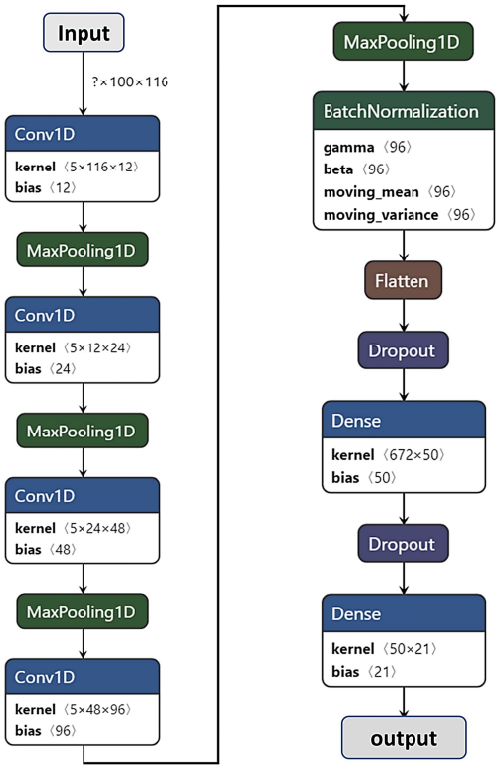

Fig. 1. Proposed CNN network architecture for gait classification. Color-coding of boxes: convolution layers and fully connected layer (blue); pooling layers (green); flattening layer (brown); dropout layers (navy); input at the top and softmax output layers (gray). The diagrams are generated using Neutron [30] from GitHub repository based on the models' weights and biases.

affects the POF sensors transmitted light intensity is affected by surface bending. This captures the specifics of foot contact and generates robust data without constraints of speed or positioning anywhere on the active surface.

C. Gait

The details of the GRF dynamics follow the gait cycle, as the 7 intervals defined by the contact of one or both feet with the walking surface (see [1], fig.1 therein). The full cycle gait intervals (events) for a single foot are: A- Heel strike or Initial contact; B- Loading response or foot flat and double support; C- Mid-stance; D- Terminal stance or Heel-off; E- Pre-swing; F- Initial swing and Mid-swing [1]. In a healthy gait cycle these 7 intervals are grouped in Stance Phase (A, B, C, D - 60% of the gait cycle, when the foot is in contact with the ground) and Swing Phase (E, F, G - 40% of the gait cycle, foot swinging and not in contact with the ground).

Further to our recent topical review [1] on gait recognition, gait recognition literature in the past two years has been focused on solving the view- and clothing invariant problem for video sequences with more advanced AI methods, such as generative adversarial network [25], [26]. Recent work on wearable and floor sensors has been applied for medical applications such as the impact of muscle fatigue on gait characteristics [27], health monitoring [28] and age-related differences [29].

III. Methodology

A. Data Acquisition and Pre-Processing

Twenty-one physically active subjects aged 20 to 40 years, 17 male and 4 females, without gait pathology or cognitive impairment, participated in this experiment. The study was carried out under the University of Manchester Research Ethics Committee (MUREC), ethical approval number 2018-4881-6782. All participants were informed about the data recording protocol in accordance with the ethics board general guidelines and each subject written consent was obtained prior to experiments. Each participant was asked to walk normally, or while performing cognitively demanding tasks, along the 2 m length direction of the iMAGiMAT sensor head. The captured gait data is unaffected by start and stop, as it is padded on both ends with unrecorded several gait cycles before the first footfall on the sensor. With a capture rate of 20 timeframes/s (each timeframe comprising the readings of all 116 sensors), experiments yielded 5s long adjacent time sequences, each containing 100 frames. The recorded gait spatiotemporal signals were able to capture around 4 to 5 uninterrupted footsteps at each pass.

Five manners of walking were defined as normal gait plus four different dual tasks, and experiments were recorded for each subject, with 10 gait trials for each manner of walking in a single assessment session; thus the total number of samples is $10 \times 5 = 50$ per-subject. The five manners of walking are defined as follows:

- Manner 1, Normal Gait: walking at normal self-selected speed.
- Manner 2, Gait while listing to a story: audio input through headphones, then answer questions after gait recording is completed.
- Manner 3, Gait with serial 7 subtractions: normal walking speed attempted, while simultaneously performing serial 7 subtractions (count backward in sevens from a given random 3-digit number).
- Manner 4, Gait while texting: normal walking speed attempted, while simultaneously typing text on a mobile device keyboard.
- Manner 5, Gait while talking: walking at normal self-selected speed while talking or answering questions.

A set of measured data as $x_{n,s} = [\, x_{n,1} \quad \dots \quad x_{n,116} \,] \in \mathbb{R}^{n \times 116}$ is harvested from the iMAGiMAT system, where n is the number of the data block (100 frames) and s enumerates the POF sensors. A total number of 1050 samples are recorded for 21 subjects and placed in a 3D matrix of dimensions $1050 \times 100 \times 116$. The recorded amplitude of data varies due to the weight of each subject, therefore, data standardization is implemented as a pre-processing step, to ensure that the data is internally consistent, such that the estimated activations, weights, and biases update similarly, rather than at different rates, during the training process and testing stage. The standardization involves rescaling the distribution of values with a zero mean unity standard deviation, using the following equation:

$$\widehat{x_{n,s}} = \frac{x_{n,s} - \mu(x_{n,s})}{\sigma(x_{n,s})} \tag{2}$$

Here $\widehat{x_{n,s}}$ is gait data rescaled so that μ is the mean and $\boldsymbol{\sigma}$ is the standard deviation.

B. CNN Structure

Gait analysis in this study is handled as a supervised learning process. Here, we propose a CNN model, based on extensive experimentation with different algorithms and architectures in our previous work [31]–[34], as automatic feature extractor and classifier. The model shown in figure 1 maps the gait spatiotemporal signal $\widehat{x_{n,s}}$ to an output label y by learning an approximation function $y = f\left(\widehat{x_{n,s}}\right)$. The network consists of an input layer, 4 convolution layers, 4 pooling layers, 2 fully connected layers, 1 batch normalization, and an output layer with a softmax classifier. The set of 12 stacked layers in figure 1 utilizes Conv1D kernels (filter size $\times$ number of feature maps $\times$ number of filters), MaxPooling strides of 2 and pool size of 2.

The network total parameters are 71,669, with 71,477 trainable and 192 non-trainable parameters. The parameters can be calculated from figure 1 as $71,477 = \sum \text{kernels} + \text{bias}$. A stride of 1 and the same padding is used in the convolutional layers to output the same length of the original input shape. To improve the model performance, a regularization method is utilized as follows: (1) Batch normalization (to normalize the activations of the previous layer at each batch, by maintaining the mean activation close to 0 and the activation standard deviation close to 1 [35]). (2) The Batch normalization followed by a dropout [36] of size 0.5, after the last MaxPooling layer was flattened, by transforming a matrix to one single column vector. (3) Dropout of size 0.2 before the output layer.

An ADAM [37] (A Method for Stochastic Optimization) is utilized to train the model. The used optimizer parameters are $\alpha = 0.002$, $\beta 1 = 0.9$, $\beta 2 = 0.999$, $\varepsilon =$ 1e-08. Here α is the learning rate or the fraction of weights updated; $\beta 1$ and $\beta 2$ are the exponential decay rates for the first and second moment estimates, respectively; ε is a small number to avoid division by zero. The loss is computed using categorical cross-entropy in every iteration to minimize the network error [38]. The convolutional layers weight parameters are initiated with a Glorot uniform [39] with zero bias. The model is trained and validated (for several experiments) using a batch size of 100 samples for each iteration; 200 epochs are found optimal to train the model. The training and validation sizes are set to be 70% and 10% respectively, where 20% is reserved for testing the model accuracy. The model is trained, validated, tested for several runs with data split using a *random state* parameter of 42, 100, 200, 2020. The mean performance and standard error are used to report the accuracy as follows

$$SE = \frac{\sqrt{\frac{\sum (F-\mu)^2}{q}}}{\sqrt{q}} \tag{3}$$

Here F *is* the F1 score, μ is the F1 scores mean and q is the number of F1 scores accuracies. The numerator is the standard deviation.

C. LRP

In this paper the POF sensor spatiotemporal signal $\widehat{x_{n,s}}$ is learned by the CNN model to make a prediction of gait class c using a classification function $f_c(x)$. This function can be interpreted as a "heat map", or relevance scores, to quantify certain signal changes associated with gait intervals. The interpretation of this function is achieved by decomposing the classification decision into regions of relevance contributed to the model classification scores. This approach is known as LRP [40], which is based on backpropagated quantity preserved between intermediate nodes of adjacent layers. The LRP produce a heat map identical to the original spatiotemporal signal $\widehat{x_{n,s}}$, which can be overlaid on the original signal to highlight the contributions of gait intervals to the CNN model prediction of gait class. As the CNN consists of stacked layers, each layer has feature maps and can be treated as neurons, where neurons are activated according to [40]:

$$a_j^{1+l} = \sigma\left(\sum_i g_{ij} + b_j^{(l+1)}\right) \tag{4}$$

with $g_{ij} = a_i^l \omega_{ij}^{(l,l+1)}$

The sum is computed over all previous layer neurons that are connected to neuron j, where a_i^l denote the activation of a neuron i in the previous layer in forward direction, and g_{ij} denote the contribution of neuron i in layer l to the activation of the neuron j in layer $l+1$. The neuron weight $\omega_{ij}^{(l,l+1)}$ is received in forward direction by neuron i from neuron j in the previous layer and $b_j^{(l+1)}$ is a bias term. The function σ is a nonlinear monotonously increasing activation function to define the output of that node given an input, ReLU = max(0, x) passing only positive signals. During CNN supervisory training, these parameters are learned by computing the output $f_c(x)$ based on evaluating a_j^{1+l} in a forward pass and updated by back-propagation using the model error. For the latter, computations are based on categorical cross entropy [38]. The LRP approach utilizes the CNN output f_c for input $x_{n,s}$ and generates a "relevance score" R_i^l for the i^{th} neuron of layer l and R_j^{l+1} from the j^{th} neuron in layer $l+1$, where the relevance conservation principle is satisfied as [41]:

$$\sum_i R_{i \leftarrow j} = \sum_j R_j = f_c(x) \tag{5}$$

IV. Experiments and Results

A. Overview

All algorithms for LRP computation are implemented in Python 3.7.3 programming language using Keras 2.2.4 [42], TensorFlow 1.14.0 and iNNvestigate GitHub repository [43]. All codes are run using a desktop with intel core i7 6700 CPU @3.4 GHz. After data standardization, the deep CNN model is applied on the dataset in order to test the validity of the algorithms for identifying gait signatures. We compared the CNN predictions to manually labelled ground truth in several experiments, based on individuals' identity and the changes to normal gait incurred by cognitive load. The models' classification performance is evaluated using confusion matrices. The performance of the LRP methods is examined in detail in subsection D.

B. Gait Signature Classification

The proposed model is trained, validated, and tested on $K \times n \times s$ (K = number of samples, n = number of frames,

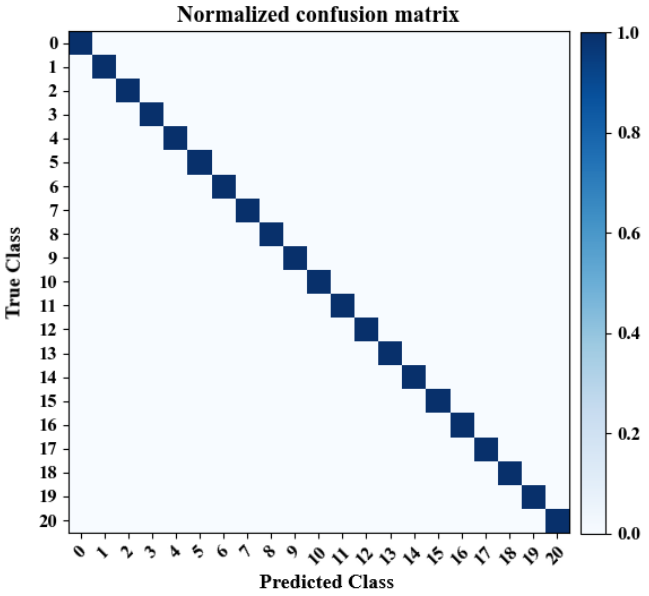

Fig. 2. Gait signature classification confusion matrix for 21 subjects. The diagonal squares are the true positives, in this case 100% of classification and elsewhere are the false positives (0%).

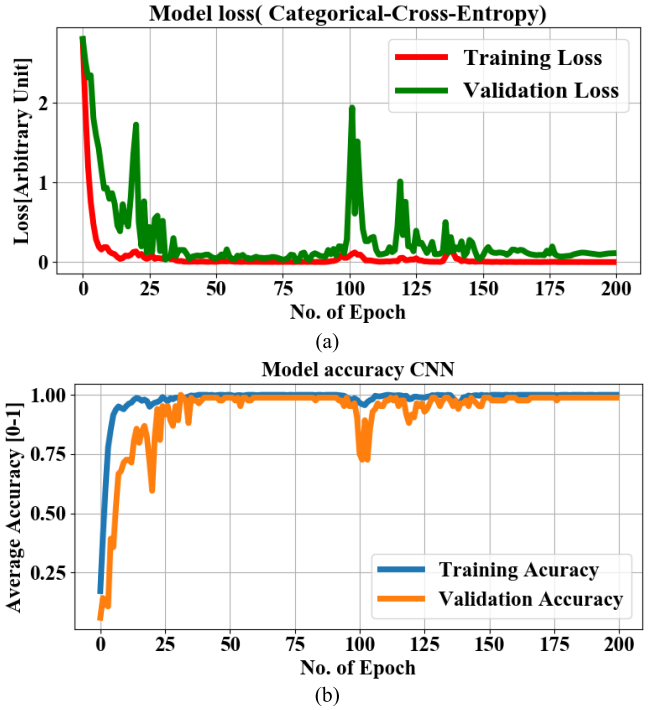

Fig. 3. Model training and validation loss in (a) and model accuracy in (b) for 21 subjects in 5 classes.

S = number of POF sensors) spatiotemporal samples as $K \times 100 \times 116$ for several runs using different *random state* parameters. K is chosen on the basis of experimental protocols and the mean performance and standard error are used to calculate the accuracy.

Experiments are conducted to investigate the ability of the deep CNN to identify gait signature patterns by fusing 116 POF sensors in the model's deep layers, to extract gait patterns automatically in the following experiments.

Experiment 1 (21 Subject Gait Signature Verification): To demonstrate the model's ability to verify the identity of a subject based on their gait signature, we assigned each subject's data a label numbered from 0 to 20, containing 50 samples of normal and cognitive load as explained in section II.D. The model is trained, validated and tested on K = 1050 samples with different *random state* parameters, and the mean performance and standard error are used to calculate the accuracy. The median classification confusion matrix is shown in figure 2, where the model achieved F1-score of 100% prediction and mean performance and standard error of $99.5 \pm 0.28\%$.

Figure 3 demonstrates the learning curve performance of the CNN over the iterations while training. We generate the training loss for each of the training sets and validation loss for each of the validation sets over the epochs. Figure 3a shows the average training and validation losses. The training loss starts from 3 and gradually reduces to 0. The validation loss generally follows the training loss, with a few spikes, and stablizes after 150 epochs. As expected, accuracy increases with decreasing loss, demonstrated in figure 3b. The average training and validation accuracy stablizes after 150 epochs after a few spikes.

For additional testing of the model performance in real-life scenarios, we evaluate the model on imposter and client classification. The client's data are used for the model training and validation and only 20% of that data is used for testing, while the imposters data are only used at the testing stage. The model at the testing stage predicts the client's gait sample identity with an F1 score of 100% and unable to predict the imposter which returns 0% F1 score. This is achieved by taking 17 subjects as clients (K = 850 samples), and 4 subjects as imposters (K = 200 samples). Clients were split 70%-10%-20% for training validation and testing respectively. In the testing stage, the model was able to distinguish correctly imposters and clients in 100% of cases.

Experiment 2 (Gender Classification): To demonstrate the model ability to recognize gait signatures, we perform a two-class classification based on the gender of the subject using the normal gait and cognitive load samples. The model is trained and validated with 6 subjects (K = 300 samples) including 3 males and 3 females. Model testing is by predicting the gait class of two new subjects (K = 100 samples, never seen by the model), the selection of males and females are done randomly. In this experiment the deep CNN prediction achieved F1-score of 95%, with 96% true positive prediction for the male samples, and 94% true positive prediction for the female samples.

Experiment 3 (21 Subjects Cognitive Load Classification): The aim of this experiment is to show that in healthy subjects the influence of cognitive load on gait varies from subject to subject and the normal gait can be predicted with higher true positive rates than predictions under cognitive load. Five types of gait signatures, normal and four cognitively demanding task patterns, are learned for 21 subjects. The performance observed for the 5 classes is shown in figure 4, as the median

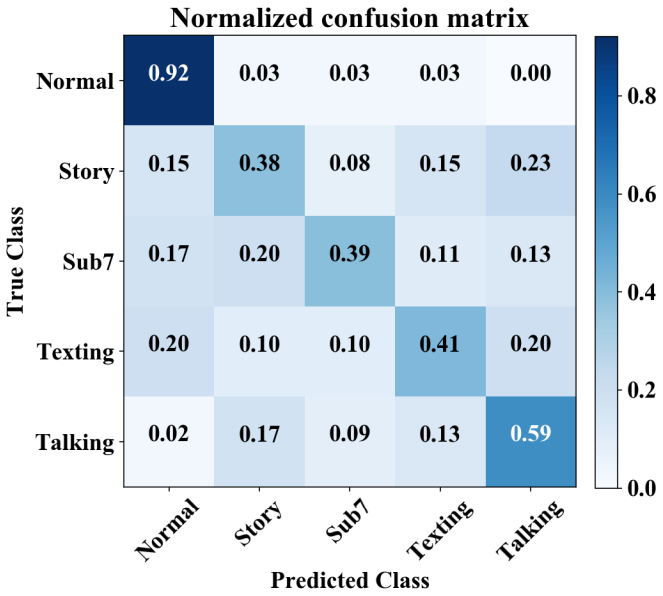

Fig. 4. Confusion matrix for classification under cognitive load: 21 subjects, 5 classes.

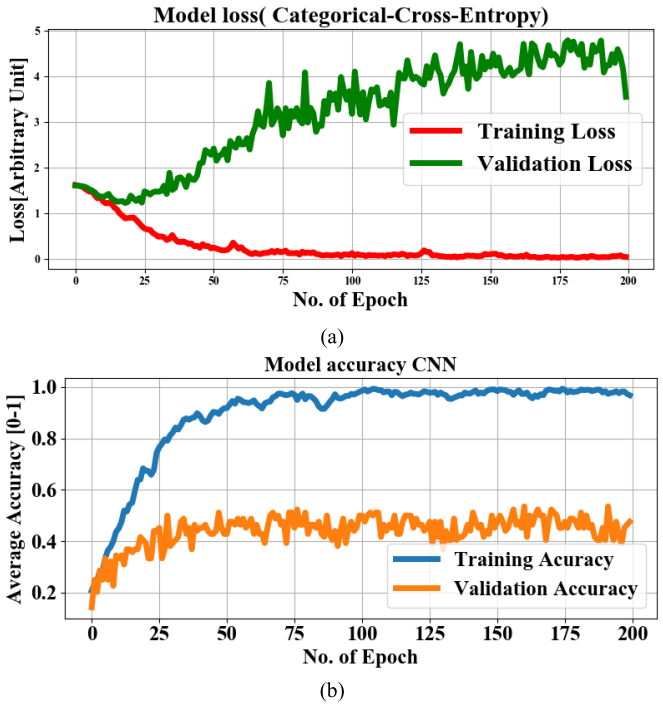

Fig. 5. Model loss (a) and training and validation accuracy (b) under cognitive load, 21 subjects and 5 classes.

confusion matrix based on several runs with F1-score of 50% and mean performance and standard error of 48.25 ± 1.03%. The results show that normal gait is predicted by a true positive incidence of 92%, while there is notable confusion between the dual tasks performed by the 21 subjects. The different *random state* parameters return the same result, where the normal gait true positive prediction is higher than 90% and substantial confusion between the dual task cases. Figure 5 shows the CNN learning curves over the training iterations, where the

TABLE I
MODELS CLASSIFICATION ACCURACY FOR EACH SUBJECT

Subject number	F1- score	Subject number	F1- score	Subject number	F1- score
0	95%	7	87%	14	100%
1	65%	8	90%	15	75%
2	93%	9	90%	16	80%
3	90%	10	77%	17	100%
4	87%	11	91%	18	100%
5	91%	12	90%	19	80%
6	73%	13	100%	20	69%

TABLE II
F1-SCORE PREDICTIONS FOR BINARY CLASSIFICATION

Data Group for Classification	1 testing subject	2 testing subjects	4 testing subjects	Test with all subjects
Class 0 vs class 1	100%	85%	81%	79%
Class 0 vs class 2	95%	87%	58%	69%
Class 0 vs class 3	60%	68%	63%	79%
Class 0 vs class 4	100%	85%	74%	81%

training loss declines from 1.8 to 0 while the validation loss rises from 1.8 to around 4 for 200 epochs, resulting in low validation accuracy as per figure 3b to evidence severe overfitting.

Experiment 4 (Single Subjects Cognitive Load Classification): In this experiment gait patterns are investigated within each subject, to show that each subject gait under cognitive load can be learned and predicted. This is achieved by training, validating, and testing the CNN to classify each subject gait pattern using the normal gait and cognitive load. Each subject data is split using *random state* of 62 to cover all the 5 classes for testing with K = 50 samples. The model evaluation using the F1- score is detailed for each subject in table I. Gait data is predicted with more than 85% F1-score for 16 subjects, and for 6 subjects F1-scores are between 65% and 77%.

Experiment 5 (Binary Classification Under Cognitive Load): To study patterns for each of the 4 dual tasks (M2-M5) representing variants of cognitive load, we organize the data into four groups so that binary classification performance to distinguish between gait under normal (class 0) and cognitive load (one of classes 1, 2, 3 or 4, depending on the particular data group) conditions can be studied separately for each dual task. The CNN is trained 16 times, implementing 4 runs with each of the 4 data groups. The F1-scores for each run are shown in table II. The first run in each data group is based on training and validating the CNN on 20 subjects and test the model on 1 subject. In the second run, the numbers are 19 and 2, respectively; in the third – 17 and 4 respectively. The last run is based on splitting the data into 70% for training, 10% for validation and 20% for testing, using K = 420 samples with 200 *random state* parameters (since the accuracy doesn't change with the *random state*). As shown in table II, the highest classification performance is achieved in the first runs (except for the group containing class 3). This is used essentially in the implementation of LRP to analyze the gait classes for that subject in the first run, as reported further.

TABLE III
F1-SCORE PREDICTIONS FOR COMPRESSION OF CNN WITH CLASSICAL CLASSIFIERS

Classifier	Experiment 1	Experiment 3
SGD	77%	42%, N=47%
KNN	87%	51%, N=81%
GPC	5%	22%, N=0%
CNN	100%	50%, N=92%

N: True positive prediction of normal gait.

C. Comparison With Statistical Classifiers

Gait signature recognition achieved high accuracy compered to Cognitive Load Classification; therefore, the validity of these achieved classification is verified with statistical classifier. Here we compare the classification results achieved by CNN in experiment 1 and 3 with statistical classifier algorithms (also known as shallow learning), such as Stochastic Gradient Descent (SGD) [44], K-Nearest Neighbors (KNN) [45], and Gaussian Process Classifier (GPC) [46]. To change the format of the statistical classifiers input, the data are flattened to length $11600 = 100 \times 116$, with and samples of $k = 1050$ for experiment 1 and 3. The classification F1-scores on experiment 1 and 3 are shown in Table III. GPC fails in the true positive prediction of normal gait, while KNN achieves the best classification results. However, the CNN outperforms the statistical classifiers for both gait signature recognition and normal gait prediction.

D. LRP Analysis of Gait Spatiotemporal Classifications

The focus of this section is to identify the features picked up by the model to classify gait under cognitive load. To obtain accurate LRP relevance scores Ri, the model true positive prediction should be high. Therefore, the gait class with high positive rate is considered for LPR analysis. The learned CNN model parameters in experiment 1, 3 and 5 were frozen for LRP analysis. Experiment 4 is to check if there is a variation in gait within a subjects; therefore it is not considered for LRP analysis. LRP Sequential Preset a Flat (LRP-SPF) [47] based on the LRP (see III.C) was utilized for this work, as it has shown sensitivity to gait inconsistency using perturbation [34].

The iMAGiMAT system captures a sequence of periodic events as distinct, but similar cycles for each foot. This spatiotemporal sequence is generated by the change of light transmission intensity in the POF sensors: $x_i = [\, x_1 \quad \ldots \quad x_{116} \,] \in \mathbb{R}^{n \times 116}$. However, a typical interpretation of the gait cycle, based on visual observation, is derived much less from the spatial component than the temporal one [1]. Thus to progress towards interpreting the CNN classifications in terms of observable gait events, we average over the spatial domain according to:

$$SA[n] = \frac{1}{s} \sum_{s=1}^{116} (x_{n,s}) \tag{6}$$

Here $x_{n,s}$ are the readings from individual sensors s at a specific frame n within each sample and SA is the frame n spatial average calculated as the arithmetic mean over all sensors. Figure 6 displays a typical SA of the spatiotemporal gait signal, labelling the main gait events [1] over a two-step gait cycle.

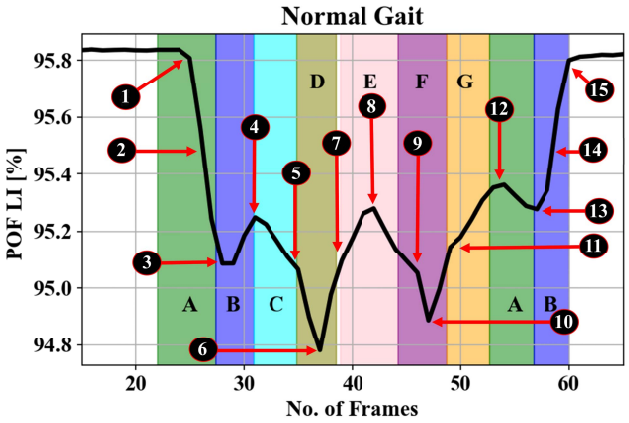

Fig. 6. Representative gait cycle spatial average of a spatiotemporal signals (see equation 6). Gait events recorded by the sensors in a typical full gait cycle of two steps ([1] as A, B, C, D, E, F, G): 1- Heel strike, 2- Foot-flattening, 3- Single support, 4- opposite Heel strike, 5- opposite Foot-flattening, 6- Double support, 7-Toe-off, 8- Foot swing, 9- Heel strike, 10- Double support, 11- Toe-off, 12- Foot swing, 13- opposite Heel strike, 14- Single support, 15-Toe-off.

Figures 7 and 8 display randomly chosen samples of single subjects, returning 100% true positives prediction for gait signature verification in experiment 1; figure 9 displays randomly selected samples of normal gait classified with 100% true positives in experiment 3; figure 10 shows predicted gait samples in experiment 5 for a subject never seen by the model when the training set is 20 subjects.

The top panels in figures 7, 8, 9 and 10 display calculated SA aligned against the relevance "heat map", generated from the calculated LRP scores and displayed in the bottom panels (to be discussed further in section V). The SA temporal sequences have different values on the y axis due to the nature of the captured gait signal, which is influenced by the individual anthropometry of subjects.

V. DISCUSSION

A. Classification of Gait Signatures Under Cognitive Load

The present study investigates the importance of cognitive load influence for gait inconsistency. We present a comparison of classification performance between 5 types of gait: normal and under cognitive load in 4 different tasks. Deep CNNs not only outperform, unsurprisingly, the classical classifier methods but also achieve an F1-score of 100% (see figure 2 and table III) for gait signature verification in experiment 1 with 21 healthy adult's data, and 100% prediction of 4 imposters and 17 clients. The learning curve in figure 3 demonstrates the good match of the CNN methodology for gait verification tasks. The network parameters are updated via backpropagation to map gait during training to 21 classes are correctly optimized at the validation stage, which is important for the testing stage to make prediction for gait verification.

Experiment 2 is in essence an extra validation of the adequacy of the spatiotemporal sampling of GRF by the

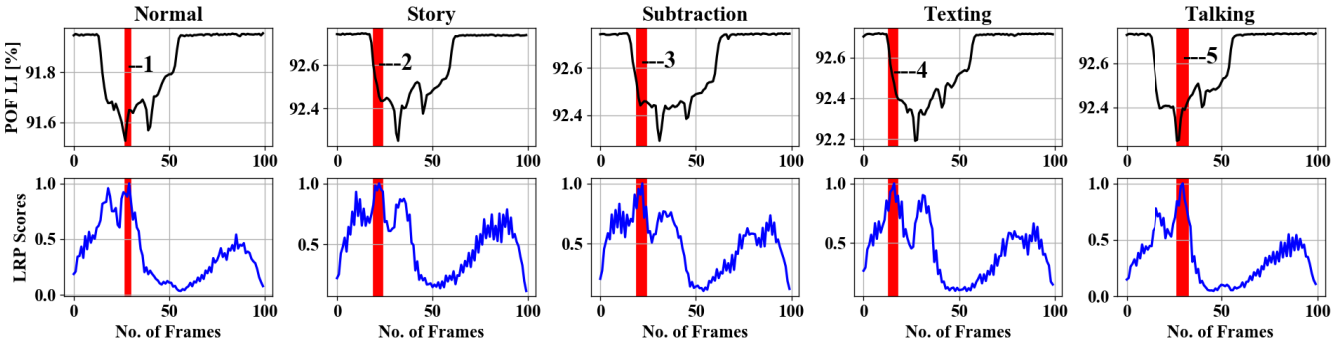

Fig. 7. LRP methods applied on a single subject from experiment 1 testing data (each column is one pair), to identify gait events relevant for the CNN prediction to classify the cognitive load impact on gait. *SA* of gait spatiotemporal signals: black; *SA* for LRP relevance signals over gait temporal period: blue; POF LI (Plastic Optical Fiber Light Intensity). Vertical red bars with numbers display correspondence to gait events as per fig. 6: 1,5- Loading response or Foot flat and Double support, 2,3,4 - Loading response or Foot flat and Single support.

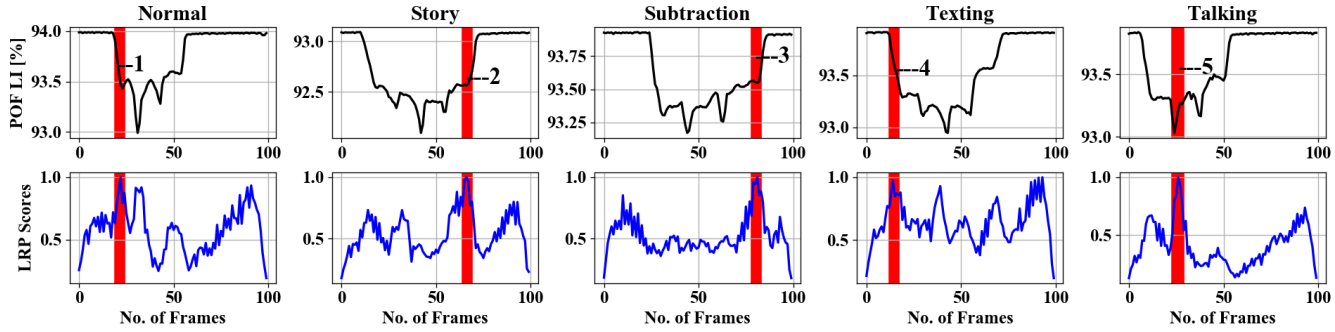

Fig. 8. Consistent with identifying gait events relevant for the CNN prediction, random subject from experiment 1 gait events are: 1,4- Loading response or Foot flat and Single support, 2,3- Foot swing and opposite Heel strike, 5- Loading response or Foot flat and Double support.

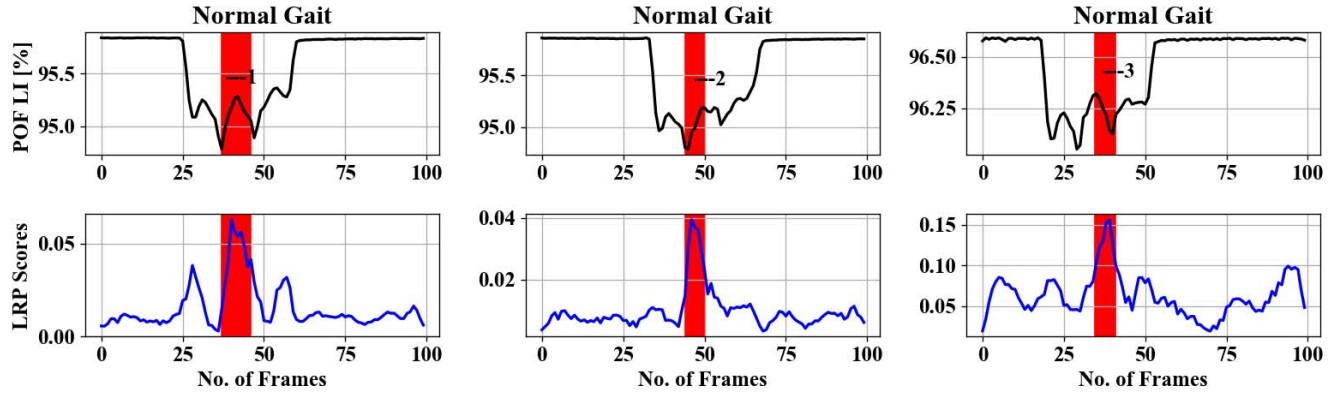

Fig. 9. LRP methods applied on normal gait samples (from different subjects) from experiment 3 testing data, to identify gait events relevant for the CNN prediction to classify the cognitive load impact on gait. Gait events are: 1, 2, 3- loading response or Foot flat and Double support.

116 sensors and their fusion, as well as that the classification performance of the trained models. An F1-score of 95% is achieved for test data from an unseen male as well as an unseen female. Although experiment 2 has the character of a sanity check, the results lend support to the value of floor sensor gait data as a biometric.

Experiment 3 is conducted to study the possibility to classify cognitive load on healthy subjects. It has shown that normal gait is classified with higher true positive rate compared to any of the cases of gait under cognitive load. This experiment also indicates that the achieved true positive rates in predicting normal gait are higher for the CNN model compared to the classical classifiers (see figure 4 and table III). The learning curve in figure 5 indicates overfitting [48], to imply that the gait patterns under cognitive load diverge among the 21 subjects. Samples obtained under cognitive load samples are hard to fit due to the inconsistency of gait pattern changes among the subjects.

The results from the first three experiments suggest that while the dual-task data obviously contributes to the high F1-scores in experiments 1 and 2, it results in substantially degraded true positive rates in experiment 3. However, experiment 4 shows that when classifications are within a single subject the performance is notably better: for 16 subjects

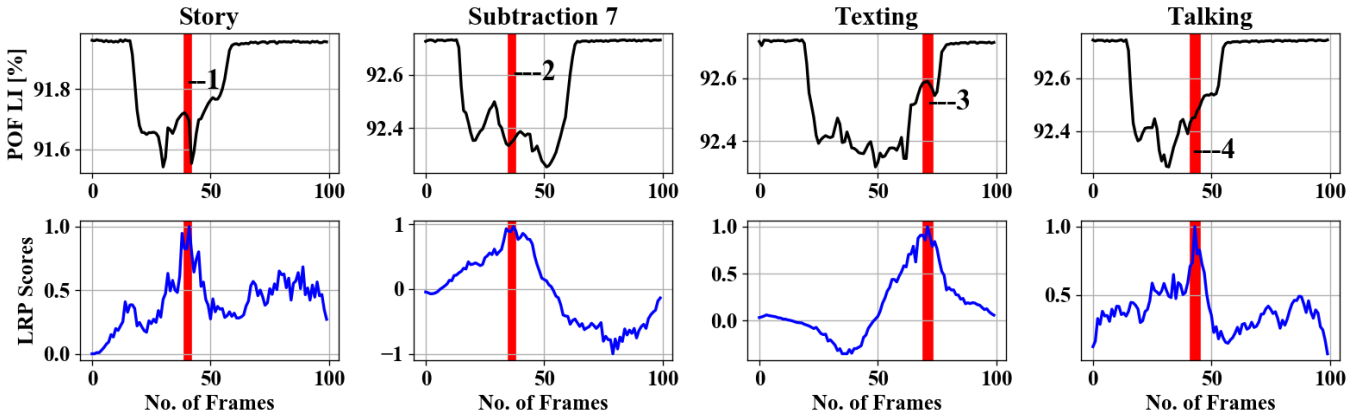

Fig. 10. LRP methods applied on a single subject from experiment 5 testing data (each column is one pair), to identify gait events relevant for the CNN prediction to classify the cognitive load impact on gait. Gait events are: 1- Heel strike, 2- Toe-off, 3- between Foot swing and opposite Heel strike, 4- between Double support and Toe-off.

(out of 21) the gait under cognitive load the F1 score ranges between 80 to 100%, with the remaining 5 subjects the range being between 69% to 77%.

These observations can be discussed in the light of humans having a natural gait pattern evolved over millions of years; however, changes in gait when experiencing cognitive load at any particular instance are specific to the individual, expressing their response to the impaired ability to process cognitive information. In experiment 5, we use binary classifications (see table II) to distinguish normal gait from gait under the 4 variants of cognitive load. The best classification results are obtained when the model learns normal or dual-task gait features for a single subject. This implies that although learned gait features under cognitive load may not be readily portable across subjects, they are consistent for each individual and can contribute substantially for correct subject classifications; however, the accuracy drops if more subjects are involved.

B. Interpretation of Classifications

Figures 7, 8, 9 and 10 provide the link between the LRP relevance scores ("heat map") and the time sequence of the calculated *SA* signal in a single gait cycle window. The LRP score maxima are suitable pointers to the parts of the gait cycle which are most relevant for the classifications. For accurate heat maps the model's true positive prediction must be close to 100% for most of the testing samples, which points to the results from experiment 1 (figures 7 and 8), experiment 3 for normal gait heat maps - in figure 9 and experiment 5 for a single subject predicted gait under the 4 variants of cognitive load - in figure 10. Focusing just on one complete gait period (two steps) is justified by the fact that on multiple repetitive occasions each subject will initiate a gait cycle (see full description of the gait cycle events in [1]) by performing a heel strike, strictly followed by other gait events described in figure 6 and ending in a toe off.

Figure 7 indicates that loading response has high relevance to assigning a gait signature to one out of the 21 subjects gait samples, notably even under cognitive load, as indicated by with gait events numbered from 1 to 5. Figure 8 shows another subject randomly selected out of the 21. The indicated gait events are loading response for normal gait (1), gait while texting (4) and gait while talking (5); Foot swing and opposite Heel strike for gait while listening to a story (2) and while performing subtraction (3). The indication of events numbered 1, 2, 3 on figure 9 implies that normal gait identified by loading response or Foot flat and double support for 21 subjects. This gait event is marked by the model by 92% true positive (see figure 4) to distinguish normal gait from 4 cognitive load classes. Figure 10 shows cognitive load gait samples for one subject as per experiment 5 (the one subject never seen by the model) summarized as follows:

i. Gait while listening to story: Heel strike is significant for distinguishing listing to story from normal walking.
ii. Gait while performing serial 7 subtraction: Toe-off is significant for distinguishing 7 subtraction from normal walking.
iii. Gait while texting in smart phone: the transition from foot swing to opposite Heel strike is significant for distinguishing texting from normal walking.
iv. Gait while talking: the transition from double support to Toe-off is important to distinguishing talking from normal walking.

Overall, the LRP analysis indicates that subjects' normal gait is characterised by loading response; while the other cognitive load gait classes is classified by landing or lifting the feet on/from the surface of the iMAGiMAT system. For subject verification there are many second relevant scores are used to predict the identity of the subject based on gait signature.

C. Benefits and Limitations

In view of gait recognition methods, floor sensors capture high resolution spatiotemporal data of gait, which is adequate for the monitoring of gait and walking habits in a range of applications. An unobtrusive floor sensor, such as iMAGiMAT, avoids the limitations caused by clothing conditions and viewing angles in video sequences [25], [26], the format of the captured signals in wearable sensors [27] and motion capture systems [49], acoustic noise background in footstep sound capturing systems [3], or the small area and fixed position

of force plates [6]. Substantially, when processed by deep learning methods, floor sensors gait data, when captured under cognitive load, allows the accurate identification of subjects. This is suitable for laboratory as well as home/dwelling use, for healthcare or security, without compromising privacy. Scaling-up and large area deployment is naturally limited by cost; however the technology demonstrated in iMAGiMAT allows the cost of materials for manufacturing the sensor head to be kept below 150 USD/sq.m [17].

VI. Conclusion

We have shown that floor sensors and gait under cognitive load can be used for subject's identifications by capturing the changes in the individual's unique gait signature due to the need to process additional cognitive information in performing additional ("dual") tasks. We have shown that, despite higher identification of subjects, gait under cognitive load is variable among healthy subjects, thus normal gait still consistence. In particular, LRP analysis of gait classifications indicate a possible bridge between the output of artificial intelligence systems for processing of high quality gait data and decisions based on visual observations by humans, or quantitative parameters derived from such observations [1], typical in current practice. An obvious potential impact is in the areas of biometrics and security [6], with the usual caveats pertaining to the regular update and fine-tuning of models, e.g. similar to other areas of biometric recognition. In healthcare alone, gait data from floor sensors can contribute and enhance the already significant interest in the detection of the onset of Parkinson disease [16] and fall risks [14]. It can be speculated that a possible future direction may involve the inobtrusive sampling of subjects' gait under routine conditions over intervals spanning periods of physical and mental changes due to ageing. Analysis of such longitudinal gait data, possibly corrected for mood, emotional state, and cognitive load personalized influences on gait, could contribute to earlier detection of disease onset.

References

[1] A. S. Alharthi, S. U. Yunas, and K. B. Ozanyan, "Deep learning for monitoring of human gait: A review," *IEEE Sensors J.*, vol. 19, no. 21, pp. 9575–9591, Nov. 2019, doi: 10.1109/JSEN.2019.2928777.

[2] S. Li, B. Schouten, and M. Tistarelli, "Biometrics at a distance: Issues, challenges, and prospects," in *Handbook Remote Biometrics* (Advances in Pattern Recognition), M. Tistarelli, S. Li, R. Chellappa, Eds. London, U.K.: Springer, 2009, pp. 3–21.

[3] Y. Shoji, T. Takasuka, and H. Yasukawa, "Personal identification using footstep detection," in *Proc. Int. Symp. Intell. Signal Process. Commun. Syst. (ISPACS)*, Nov. 2004, pp. 43–47, doi: 10.1109/ISPACS.2004.1439012.

[4] A. Elkholy, M. E. Hussein, W. Gomaa, D. Damen, and E. Saba, "Efficient and robust skeleton-based quality assessment and abnormality detection in human action performance," *IEEE J. Biomed. Health Informat.*, vol. 24, no. 1, pp. 280–291, Jan. 2020, doi: 10.1109/JBHI.2019.2904321.

[5] F. Horst, S. Lapuschkin, W. Samek, K.-R. Müller, and W. I. Schöllhorn, "Explaining the unique nature of individual gait patterns with deep learning," *Sci. Rep.*, vol. 9, no. 1, pp. 1–13, Feb. 2019, doi: 10.1038/s41598-019-38748-8.

[6] O. Costilla-Reyes, R. Vera-Rodriguez, P. Scully, and K. B. Ozanyan, "Analysis of spatio-temporal representations for robust footstep recognition with deep residual neural networks," *IEEE Trans. Pattern Anal. Mach. Intell.*, vol. 41, no. 2, pp. 285–296, Feb. 2019, doi: 10.1109/TPAMI.2018.2799847.

[7] J. M. Hausdorff, A. Schweiger, T. Herman, G. Yogev-Seligmann, and N. Giladi, "Dual-task decrements in gait: Contributing factors among healthy older adults," *J. Gerontol., A, Biol. Sci. Med. Sci.*, vol. 63, no. 12, pp. 1335–1343, Dec. 2008, doi: 10.1093/gerona/63.12.1335.

[8] G. Yogev-Seligmann, J. M. Hausdorff, and N. Giladi, "The role of executive function and attention in gait," *Movement Disorders*, vol. 23, no. 3, pp. 329–342, Feb. 2008, doi: 10.1002/mds.21720.

[9] J. E. A. Bertram and A. Ruina, "Multiple walking speed–frequency relations are predicted by constrained optimization," *J. Theor. Biol.*, vol. 209, no. 4, pp. 445–453, Apr. 2001, doi: 10.1006/jtbi.2001.2279.

[10] K. G. Holt, S. F. Jeng, R. Ratcliffe, and J. Hamill, "Energetic cost and stability during human walking at the preferred stride frequency," *J. Motor Behav.*, vol. 27, no. 2, pp. 164–178, Jun. 1995, doi: 10.1080/00222895.1995.9941708.

[11] J. C. Selinger, S. M. O'Connor, J. D. Wong, and J. M. Donelan, "Humans can continuously optimize energetic cost during walking," *Current Biol.*, vol. 25, no. 18, pp. 2452–2456, Sep. 2015, doi: 10.1016/j.cub.2015.08.016.

[12] I. Birch, T. Birch, and D. Bray, "The identification of emotions from gait," *Sci. Justice*, vol. 56, no. 5, pp. 351–356, 2016, doi: 10.1016/.j.scijus.2016.05.006.

[13] A. Marengoni *et al.*, "Aging with multimorbidity: A systematic review of the literature," *Ageing Res. Rev.*, vol. 10, no. 4, pp. 430–439, Sep. 2011, doi: 10.1016/j.arr.2011.03.003.

[14] J. M. Hausdorff, D. A. Rios, and H. K. Edelberg, "Gait variability and fall risk in community-living older adults: A 1-year prospective study," *Arch. Phys. Med. Rehabil.*, vol. 82, no. 8, pp. 1050–1056, Aug. 2001, doi: 10.1053/apmr.2001.24893.

[15] Y. Barak, R. C. Wagenaar, and K. G. Holt, "Gait characteristics of elderly people with a history of falls: A dynamic approach," *Phys. Therapy*, vol. 86, no. 11, pp. 1501–1510, Nov. 2006, doi: 10.2522/ptj.20050387.

[16] R. Mc Ardle, R. Morris, J. Wilson, B. Galna, A. J. Thomas, and L. Rochester, "What can quantitative gait analysis tell us about dementia and its subtypes? A structured review," *J. Alzheimer's Disease*, vol. 60, no. 4, pp. 1295–1312, Nov. 2017.

[17] J. A. Cantoral-Ceballos *et al.*, "Intelligent carpet system, based on photonic guided-path tomography, for gait and balance monitoring in home environments," *IEEE Sensors J.*, vol. 15, no. 1, pp. 279–289, Jan. 2015, doi: 10.1109/JSEN.2014.2341455.

[18] K. B. Ozanyan, "Tomography defined as sensor fusion," in *Proc. IEEE SENSORS*, Busan, South Korea, Nov. 2015, pp. 1–4, doi: 10.1109/ICSENS.2015.7370554.

[19] K. B. Ozanyan, S. G. Castillo, and F. J. P. Ortiz, "Guided-path tomography sensors for nonplanar mapping," *IEEE Sensors J.*, vol. 5, no. 2, pp. 167–174, Apr. 2005, doi: 10.1109/JSEN.2005.843895.

[20] J. C. Ceballos, N. Nurgiyatna, P. Scully, and K. B. Ozanyan, "Smart carpet for imaging of objects' footprint by photonic guided-path tomography," in *Proc. IEEE Africon*, Victoria Falls, Zambia, Sep. 2011, pp. 1–6, doi: 10.1109/AFRCON.2011.6071986.

[21] W. Samek, G. Montavon, A. Vedaldi, L. K. Hansen, and K. R. Müller, *Explainable AI: Interpreting, Explaining and Visualizing Deep Learning* (Lecture Notes in Computer Science). Cham, Switzerland: Springer, 2019, doi: 10.1007/978-3-030-28954-6.

[22] C. Seibold, W. Samek, A. Hilsmann, and P. Eisert, "Accurate and robust neural networks for security related applications exampled by face morphing attacks," 2018, *arXiv:1806.04265*. [Online]. Available: https://arxiv.org/abs/1806.04265

[23] L. Arras, F. Horn, G. Montavon, K.-R. Müller, and W. Samek, "'What is relevant in a text document?': An interpretable machine learning approach," *PLoS ONE*, vol. 12, no. 8, Aug. 2017, Art. no. e0181142, doi: 10.1371/journal.pone.0181142.

[24] S. Becker, M. Ackermann, S. Lapuschkin, K.-R. Müller, and W. Samek, "Interpreting and explaining deep neural networks for classification of audio signals," 2018, *arXiv:1807.03418*. [Online]. Available: https://arxiv.org/abs/1807.03418

[25] P. Zhang, Q. Wu, and J. Xu, "VT-GAN: View transformation GAN for gait recognition across views," in *Proc. Int. Joint Conf. Neural Netw. (IJCNN)*, Budapest, Hungary, Jul. 2019, pp. 1–8, doi: 10.1109/IJCNN.2019.8852258.

[26] M. Babaee, Y. Zhu, O. Kopuklu, S. Hormann, and G. Rigoll, "Gait energy image restoration using generative adversarial networks," in *Proc. IEEE Int. Conf. Image Process. (ICIP)*, Taipei, Taiwan, Sep. 2019, pp. 2596–2600, doi: 10.1109/ICIP.2019.8803236.

[27] A. Balakrishnan, J. Medikonda, and P. K. Namboothiri, "Analysis of the effect of muscle fatigue on gait characteristics using data acquired by wearable sensors," in *Proc. IEEE Int. Conf. Distrib. Comput.,*

VLSI, Electr. Circuits Robot. (DISCOVER), Udupi, India, Oct. 2020, pp. 137–140, doi: 10.1109/DISCOVER50404.2020.9278096.
[28] F. Muheidat and L. A. Tawalbeh, "In-home floor based sensor system-smart carpet-to facilitate healthy aging in place (AIP)," *IEEE Access*, vol. 8, pp. 178627–178638, 2020, doi: 10.1109/ACCESS.2020.3027535.
[29] O. Costilla-Reyes, P. Scully, I. Leroi, and K. B. Ozanyan, "Age-related differences in healthy adults walking patterns under a cognitive task with deep neural networks," *IEEE Sensors J.*, vol. 21, no. 2, pp. 2353–2363, Jan. 2021, doi: 10.1109/JSEN.2020.3021349.
[30] L. Roeder. (2020). *Netron*. [Online]. Available: https://github.com/lutzroeder/netron
[31] A. S. Alharthi, S. U. Yunas, and K. B. Ozanyan, "Sensor fusion for analysis of gait under cognitive load: Deep learning approach," in *Proc. IEEE Sensors Appl. Symp. (SAS)*, Mar. 2020, pp. 1–6, doi: 10.1109/SAS48726.2020.9220046.
[32] A. S. Alharthi and K. B. Ozanyan, "Deep learning for ground reaction force data analysis: Application to wide-area floor sensing," in *Proc. IEEE 28th Int. Symp. Ind. Electron. (ISIE)*, Jun. 2019, pp. 1401–1406, doi: 10.1109/ISIE.2019.8781511.
[33] A. S. Alharthi and K. B. Ozanyan, "Deep learning and sensor fusion methods for cognitive load gait difference in males and females," in *Proc. 20th Int. Conf. Intell. Data Eng. Automated Learn.*, 2019, pp. 229–237, doi: 10.1007/978-3-030-33607-3_25.
[34] A. S. Alharthi, A. J. Casson, and K. B. Ozanyan, "Gait spatiotemporal signal analysis for Parkinson's disease detection and severity rating," *IEEE Sensors J.*, vol. 21, no. 2, pp. 1838–1848, Jan. 2021, doi: 10.1109/JSEN.2020.3018262.
[35] S. Ioffe and C. Szegedy, "Batch normalization: Accelerating deep network training by reducing internal covariate shift," 2015, *arXiv:1502.03167*. [Online]. Available: https://arxiv.org/abs/1502.03167
[36] N. Srivastava, G. Hinton, A. Krizhevsky, I. Sutskever, and R. Salakhutdinov, "Dropout: A simple way to prevent neural networks from overfitting," *J. Mach. Learn. Res.*, vol. 15, no. 1, pp. 1929–1958, 2014.
[37] D. P. Kingma and J. L. Ba, "Adam: A method for stochastic optimization," in *Proc. 3rd Int. Conf. Learn. Represent. (ICLR)*, 2015, pp. 1–15.
[38] Z. Zhang and M. R. Sabuncu, "Generalized cross entropy loss for training deep neural networks with noisy labels," 2018, *arXiv:1805.07836*. [Online]. Available: https://arxiv.org/abs/1805.07836
[39] X. Glorot and Y. Bengio, "Understanding the difficulty of training deep feedforward neural networks," in *Proc. 13th Int. Conf. Artif. Intell. Statist.*, Y.W. Teh and M. Titterington, Eds., vol. 9. Sardinia, Italy: Chia Laguna Resort, 2010, pp. 249–256.
[40] W. Samek, A. Binder, G. Montavon, S. Lapuschkin, and K.-R. Muller, "Evaluating the visualization of what a deep neural network has learned," *IEEE Trans. Neural Netw. Learn. Syst.*, vol. 28, no. 11, pp. 2660–2673, Nov. 2017, doi: 10.1109/TNNLS.2016.2599820.
[41] G. Montavon, W. Samek, and K.-R. Müller, "Methods for interpreting and understanding deep neural networks," *Digit. Signal Process.*, vol. 73, pp. 1–15, Feb. 2018, doi: 10.1016/j.dsp.2017.10.011.
[42] F. Chollet. *The Python Deep Learning Library*. Keras. Accessed: Feb. 2021. [Online]. Available: https://keras.io/
[43] A. Maximilian *et al.* (2018). *iNNvestigate Neural Networks!*. [Online]. Available: https://github.com/albermax/innvestigate
[44] T. Zhang, "Solving large scale linear prediction problems using stochastic gradient descent algorithms," in *Proc. 21st Int. Conf. Mach. Learn. (ICML)*, 2004, p. 116, doi: 10.1145/1015330.1015332.
[45] N. S. Altman, "An introduction to kernel and nearest-neighbor nonparametric regression," *Amer. Statistician*, vol. 46, no. 3, p. 175, Aug. 1992.
[46] G. Xiao, Q. Cheng, and C. Zhang, "Detecting travel modes using rule-based classification system and Gaussian process classifier," *IEEE Access*, vol. 7, pp. 116741–116752, 2019, doi: 10.1109/ACCESS.2019.2936443.
[47] M. Kohlbrenner, A. Bauer, S. Nakajima, A. Binder, W. Samek, and S. Lapuschkin, "Towards best practice in explaining neural network decisions with LRP," 2019, *arXiv:1910.09840*. [Online]. Available: https://arxiv.org/abs/1910.09840
[48] W. Rawat and Z. Wang, "Deep convolutional neural networks for image classification: A comprehensive review," *Neural Comput.*, vol. 29, no. 9, pp. 2352–2449, Sep. 2017, doi: 10.1162/neco_a_00990.
[49] A. R. Anwary, H. Yu, A. Callaway, and M. Vassallo, "Validity and consistency of concurrent extraction of gait features using inertial measurement units and motion capture system," *IEEE Sensors J.*, vol. 21, no. 2, pp. 1625–1634, Jan. 2021, doi: 10.1109/JSEN.2020.3021501.

Abdullah S. Alharthi received the M.Sc. degree in electrical engineering from St. Mary's University, San Antonio, TX, USA, in 2015. He is currently pursuing the Ph.D. degree in electrical and electronic engineering with the University of Manchester, Manchester, U.K. From 2015 to 2017, he was with Robotics Technologies and Intelligent Systems, KACST, Saudi Arabia, as a Research Engineer. His research interests include data analysis, pattern recognition, sensor fusion, deep learning, and human gait analysis applications.

Alexander J. Casson (Senior Member, IEEE) received the M.Eng. degree in engineering science and the Ph.D. degree in circuits and systems in 2006 and 2010, respectively. His research focuses on non-invasive bioelectronics interfaces: the design and application of wearable sensors, and "conformal sensors," for human body monitoring and data analysis from highly artefact prone naturalistic situations. He is currently a Fellow of the Higher Education Academy and the Vice Chair of the Institution of Engineering and Technology's Healthcare Technologies Network.

Krikor B. Ozanyan (Senior Member, IEEE) received the M.Sc. degree in engineering physics (semiconductors) and the Ph.D. degree in solid-state physics in 1980 and 1989, respectively. He is currently the Director of Research with the Department of EEE, The University of Manchester, U.K. He has more than 300 publications in the areas of photonic materials, devices and systems for sensing and imaging. He is also a Fellow of the Institute of Engineering and Technology, U.K., and the Institute of Physics, U.K. He was a Distinguished Lecturer of the IEEE Sensors Council in 2009 and 2010, and a Guest Editor for the 10th Anniversary Issue of IEEE SENSORS JOURNAL in 2010, as well as the Special Issues on Sensors for Industrial Process Tomography in 2005 and THz Sensing: Materials, Devices and Systems in 2012. He was the Editor-in-Chief of the IEEE SENSORS JOURNAL from 2011 to 2018 and was the General Co-Chair of the IEEE SENSORS 2017 conference. He also serves as the Vice-President for publications of the IEEE Sensors Council.